

Acoustic Fluidization and the Extraordinary Mobility of Sturzstroms

Gareth S. Collins and H. Jay Melosh

Lunar and Planetary Laboratory, University of Arizona.

Abstract. Sturzstroms are a rare category of rock avalanche that travel vast horizontal distances with only a comparatively small vertical drop in height. Their extraordinary mobility appears to be a consequence of sustained fluid-like behavior during motion, which persists even for driving stresses well below those normally associated with granular flows. One mechanism that may explain this temporary increase in the mobility of rock debris is acoustic fluidization; where transient, high-frequency pressure fluctuations, generated during the initial collapse and subsequent flow of a mass of rock debris, may locally relieve overburden stresses in the rock mass and thus reduce the frictional resistance to slip between fragments. In this paper we develop the acoustic fluidization model for the mechanics of sturzstroms, and discuss the conditions under which this process may sustain fluid-like flow of large rock avalanches at low driving stresses.

1. Introduction

The downslope mass-movement of dry, unconsolidated rock material is a common geological process. Such events are often referred to as landslides, or, more correctly, rock avalanches. The mechanics of such phenomena are generally well understood in terms of the competition between gravity or inertia and inter-granular friction [for example *Carson and Kirkby*, 1972]. However, there exists a rare category of rock avalanche that travels vast horizontal distances with only a comparatively small vertical drop in height. Long-runout landslides or, more appropriately, “sturzstroms,” appear to travel as if the coefficient of friction, which usually controls the downslope motion of rock debris, is temporarily reduced by an order of magnitude or more [*Hsü*, 1975].

The fundamental law of the granular state is that a pile of granular material is stationary as long as the top surface slope is less than the “maximum angle of stability” θ_m [*Jaeger and Nagel*, 1992]. Experimental measurements of this angle show that it is a function of porosity, grain shape, amount of inter-lock between grains and material type; however, for most naturally occurring, dry-rock hillslope materials, θ_m differs by only a few degrees [for example *Carson and Kirkby*, 1972, p. 93]. Shearbox experiments to determine the frictional resistance to sliding of those same granular materials show that the shear strength f is approximately proportional to the overburden pressure p :

$$f = \mu p. \quad (1)$$

In this equation, which is most commonly referred to as Coulomb’s Law, the constant of proportionality μ is termed the coefficient of friction. Empirical evidence suggests that, for the majority of rock materials, the coefficient of friction μ is approximately 0.5–0.7 [for example *Jaeger and Cook*,

1969, p. 59] and that $\mu \approx \tan \theta_m$. Hence, both the maximum angle of stability and the coefficient of friction may be assumed to be approximately independent of material type, porosity, grain shape, gravity and overburden pressure.

The previous arguments suggest that, if one were to measure the vertical fall height H and the horizontal runout distance L for any dry rock avalanche, regardless of setting, then the ratio H/L (a commonly used proxy for the coefficient of friction, which we will call the effective coefficient of friction) should be approximately the same. However, dry rock avalanches involving more than about 10^6 m^3 of rock debris, both in a terrestrial and extra-terrestrial setting, illustrate a distinct negative correlation between H/L and avalanche volume V (see Figure 1). Least-squares fits to the terrestrial and Martian large rock avalanche data illustrated in Figure 1 give linear correlation coefficients of 0.81 for the terrestrial points and 0.9 for the Martian points. The slopes of the two trends are indistinguishable from -0.16 , hence, H/L scales as $V^{-0.16}$. However, the best-fit line for the Martian data lies above that for the terrestrial data. Clearly, these relationships cannot be explained purely by Coulomb friction—for large rock avalanches some mechanism appears to progressively lower the effective coefficient of friction with increasing avalanche volume, thereby increasing the mobility of the avalanche. Furthermore, this mechanism appears to operate differently on planets with different gravitational accelerations.

In attempting to address this issue, *Dade and Huppert* [1998] provide an adequate phenomenological explanation for the observed relationship between the effective coefficient of friction and avalanche volumes above 10^6 m^3 by assuming a constant resisting stress during runout (about 10–100 kPa), regardless of the avalanche volume and the pressure within the avalanche. *McEwen* [1989] uses a similar rheologic model for dry rock avalanches to explain the difference in the observed relationship between the effective coefficient of friction and avalanche volume on Earth and Mars. These rheologic models, which suppose that the strength of rock debris is independent of pressure, are motivated by models of plastic deformation, a common property of water-saturated

Copyright 2003 by the American Geophysical Union.

Paper number .
0148-0227/03/\$9.00

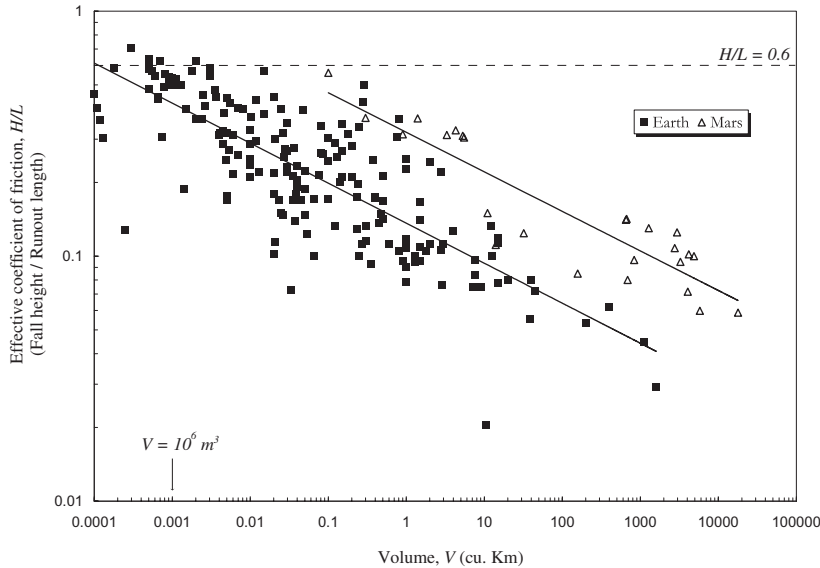


Figure 1. Graph showing the effective coefficient of friction versus avalanche volume for large rock avalanches on Earth and Mars [compiled from data in, *Hsü, 1975; McEwen, 1989; Shaller, 1991; Dade and Huppert, 1998*]. The effective coefficient of friction is the vertical drop in height H divided by the horizontal runout distance traveled by the avalanche L ; it is a measure of avalanche mobility. Most small rock avalanches have an effective coefficient of 0.6; larger avalanches, represented in the graph, show an increase in mobility (reduction in effective coefficient of friction) with increasing avalanche volume. Martian rock avalanches show the same general trend; however, the line of best fit lies above that for Earth.

soils or molten rocks. However, such a yield law is not normally associated with the deformation of dry rock debris. Furthermore, the stresses determined by *Dade and Huppert* [1998] and by *McEwen* [1989] are more than an order of magnitude less than that predicted by Coulomb friction. A fundamental question arises: how may large, dry rock avalanches adopt this type of rheology?

Historical commentary on long-runout landslides has often referred to the fluid-like behaviour of the debris [see *Hsü, 1975*]. In fact, the term “sturzstrom” (fall- or collapse-stream) derives from the earliest of these observations, which relate to the catastrophic Elm rock avalanche in Switzerland in 1881 [*Heim, 1882*]. Based on eye-witness reports and the geometrical similarity between the avalanche deposit and lava flows and glaciers, *Heim* [1882] concluded that, after an initial, violent collapse, the debris *flowed* down the slope ‘like a torrential flood.’ Geologic field mapping of large rock avalanches also suggests that, in many cases, gross stratigraphic relations in the debris mass are preserved during emplacement [for example *Shreve, 1968*].

Numerous mechanisms have been proposed to explain the low strength and fluidity of sturzstroms, for example: water or air lubrication [*Shreve, 1968*], local steam generation [*Goguel, 1978*], melt generation [*Erismann, 1979*], grain sorting [*Fineburg, 1997*], dispersive grain flow [*Bagnold, 1956; McSaveney, 1978*], acoustic fluidization [*Melosh, 1979, 1987*] and granular temperature [*Campbell, 1990; Iverson et al., 1997*]. However, the discovery of sturzstroms on the moon [*Howard, 1973*], Mars [*Lucchitta, 1978, 1979*], Venus [*Malin, 1992*], Io [*Schenk and Bulmer, 1998*], Callisto [*Chuang and Greeley, 2000*], and Phobos [*Shingareva and Kuzmin, 2001*],

certainly appears to rule out the fundamental involvement of volatiles or atmospheric gases in the flow mechanism.

The universal occurrence of the observed increase in avalanche mobility with increasing volume, regardless of geologic setting, avalanche or substrate material, presence of fluids, and so on, strongly suggests that the mechanism responsible is a fundamental mechanical process inherent to debris flows on this scale, and not peculiar to specific conditions. *Melosh* [1987] argues that the only such mechanism uniquely capable of explaining all the characteristics of sturzstroms is acoustic fluidization. The premise of this model is that large, high-frequency pressure fluctuations, generated during the initial collapse and subsequent flow of a mass of rock debris, may locally relieve overburden stresses in the rock mass. Thus, the vibrations may facilitate rapid fluid-like flow of the debris, even in the absence of large driving stresses. The purpose of this paper is to extend and quantify the acoustic fluidization model for the mechanics of large dry rock avalanches. Moreover, this paper will show that, under certain conditions, the flow of a mass of dry rock debris can retain and regenerate enough acoustic energy to perpetuate its own motion, thereby explaining the extraordinary mobility of sturzstroms.

2. Acoustic Fluidization

Although proposed over twenty years ago, acoustic fluidization is not a well-known physical process. Indeed, its peculiarity has often led to its misinterpretation. Before exploring the mathematics behind acoustic fluidization, therefore, it is important to understand the nature of the motion of acoustically fluidized debris. A mass of debris in the presence of a strong acoustic field behaves as a fluid only from

a macroscopic point of view. The law of friction between rock fragments does not change, only the pressure confining them. The random nature of the pressure vibrations means that within a small volume of the debris mass (a region smaller than the acoustic wavelength, but larger than a rock fragment) the local pressure oscillates between less-than-ambient and more-than-ambient overburden pressures. During periods when the local pressure is low enough to permit slippage, movement of the debris occurs within this small volume. At all other times the debris within the small volume remains stationary. The time- and space-averaged effect of these frequent failure events results in a creep-like process throughout the acoustically fluidized mass of rock debris. Hence, macroscopically, the debris mass appears to flow, the rapidity of which is a function of the frequency and amplitude of the failure events.

Acoustic fluidization should not be confused with the closely related process of dispersive grain flow, where motion of the debris mass generates random grain oscillations in the directions transverse to the direction of flow. Both dispersive grain flow and acoustic fluidization predict that a mass of debris may be fluidized, if the overburden pressure is relieved by random motions within the debris. However, the crucial difference is that acoustic fluidization assumes that the random movement is not that of individual rock fragments, but groups of fragments organized into waves. The concept of acoustic fluidization occupies a middle ground

between seismic-like oscillations, with wavelengths comparable to the size of the avalanche itself, and the very short wavelength oscillations associated with dispersive grain flow, which are often described as “granular temperature” [for example *Iverson et al.*, 1997]. On these short wavelength scales (wavelength comparable to the grain diameter), the motion of individual grains is uncorrelated: Collisions transfer energy and momentum from one grain to another in close analogy to a gas of molecules [*Campbell*, 1990]; consequently, energy losses are large. In acoustically fluidized debris the wavelength of these fluctuations is much longer and the motion of adjacent grains is strongly correlated, in close analogy to a liquid. Collisions are rare and gentle so that energy losses are small, while the mass of the debris still possesses a high degree of mobility.

There is now substantial support for the existence of acoustic fluidization both from engineering practice, such as vibratory pile driving [*Rodger and Littlejohn*, 1980], as well as from shake tables [*Richards et al.*, 1990] and the response of factory foundations to strongly vibrating machinery [*Barkan*, 1962]. Furthermore, some carefully controlled observations of acoustic fluidization now exist [*Gaffney and Melosh*, 1982; *Melosh*, 1983; *Zik et al.*, 1992; *Melosh and Girdner*, 1995]. In particular, *Melosh and Girdner* [1995] demonstrated that the theoretical stress-strain curve of acoustically fluidized debris is closely followed in vibrated granular materials. Moreover, recent numerical simulations of large-scale landslides [*Campbell et al.*, 1995], which predict fluid-like behaviour of the avalanche, appear to exhibit violent pressure fluctuations within the avalanche. Here we will extend the theoretical model describing the effects of acoustic fluidization on a dry rock avalanche. Before doing so, however, it is important to formally understand the mechanics of a dry rock avalanche.

2.1. The mechanics of a dry rock avalanche

Consider the stresses associated with a wide sheet of dry rock debris, thickness h , which is flowing down a slope inclined at an angle θ to the horizontal under a gravitational acceleration of g vertically down (Fig. 2).

If the avalanche is flowing in a steady state, that is, its motion does not vary with time, then the pressure gradient driving the flow in the downslope direction (x) must exactly balance the pressure gradient due to the component of gravity in the same direction, $\rho g \sin \theta$, giving:

$$\frac{dp}{dx} = -\rho g \sin \theta. \quad (2)$$

The stress equilibrium equations [for example *Jaeger and Cook*, 1969, p. 110] require that the pressure gradient in the downslope direction is balanced by the shear-stress gradient in the z -direction (orthogonal to the plane of the avalanche); $d\tau/dz$:

$$\frac{d\tau_{zx}}{dz} = \frac{dp}{dx} = -\rho g \sin \theta \quad (3)$$

so long as the slide does not accelerate.

Integrating this equation across the thickness of the avalanche, and assuming that $\tau_{zx} = 0$ at the free surface ($z = 0$), gives the shear stress in the avalanche as: $-\rho g z \sin \theta$. The negative implies that this is a resistive stress, acting to oppose the flow. Thus, the effective shear stress driving the downslope flow τ_{zx} is:

$$\tau_{zx} = \rho g z \sin \theta. \quad (4)$$

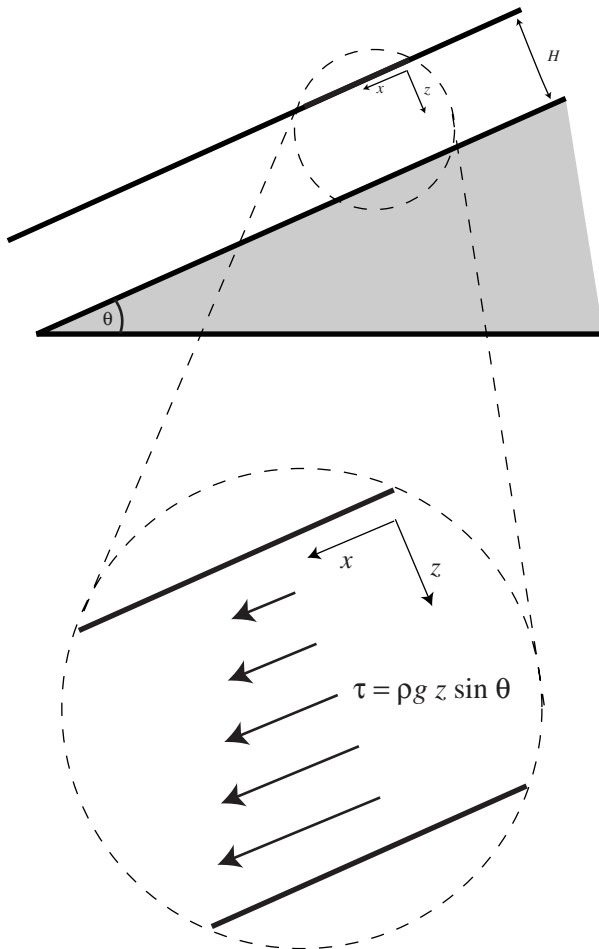


Figure 2. Schematic illustration of the stresses in a wide, thin avalanche. See text for details.

For a Coulomb material the frictional resistance is $f = \mu p = \mu \rho g z \cos \theta$; thus, the avalanche will only sustain flow if: $\tan \theta > \mu$. In other words, the dry rock avalanche will flow downslope only if the slope angle exceeds the maximum angle of stability.

2.2. The rheology of acoustically fluidized debris

The premise of acoustic fluidization is that high-frequency pressure vibrations within a debris mass counteract the ambient overburden pressure, thus reducing the frictional resistance to shear. In other words, the pressure term in Equation 1 is modified to include the effect of transient, high-frequency pressure vibrations $p_v(x, y, z, t)$, giving $f = \mu(p + p_v)$. This process is conceptually similar to the mechanism of pore-pressure variation in wet, flowing debris, as described by *Iverson et al.* [1997].

A new addition to the original derivation of acoustic fluidization [*Melosh*, 1979] was suggested by laboratory experiments in which dry sand was fluidized by strong vibrations [*Melosh and Girdner*, 1995]. In these experiments the rheology of the vibrated sand was measured as a function of the applied stress and the amplitude of the vibrations. Good agreement was found with the predicted rheological relationship [*Melosh*, 1979], with the proviso that the effective elastic modulus was much lower than that measured independently from compressive wave speeds. The reason for this apparent low modulus (which implies a much higher strain rate than expected) was suggested by high-resolution video images of the shearing layer. These images showed that the shearing material was in an expanded, dilatent state. Under these conditions, the effective shear modulus is much lower than the compression modulus [*Lambe and Whitman*, 1979].

The fundamental equation for the strain rate in acoustically fluidized material is that the average strain rate $\dot{\epsilon}$ is equal to the amount of elastic strain released each time the overburden stress falls below the value needed to produce sliding (effectively the shear stress τ divided by the shear modulus G), times the rate of such strain release events, given by the probability that the amplitude of the wave rarefaction exceeds the critical limit, $P(p > p_c)$, times the frequency of the wave, $f = c_p/\lambda$, where c_p is the speed of the dominant compressive wave. Thus,

$$\dot{\epsilon} \approx \frac{\tau c_p}{G \lambda} P(p > p_c). \quad (5)$$

The original derivation implicitly assumed that the shear modulus G was similar to the bulk modulus K , and thus that $G = \rho c_p^2$. In most solid materials this is probably true to within a factor of 2 to 4, but in actively shearing granular materials this is a poor assumption. Figure 3a illustrates the difference between actively shearing, dilatent materials and close-packed, dense granular materials. Figure 3b schematically illustrates the difference in the stress/strain behavior of these two granular states. In the actively shearing material there is little resistance to further deformation; grains, already separated by previous shear episodes, easily slide over one another. The effective shear modulus, given by the slope of the dashed line in Figure 3b, is small. In closely packed material, the grains must move up and over one another before significant strain can accumulate. The strength of such a mass is high and the effective shear modulus is large. Figure 3b also shows that, as strain accumulates and the material dilates, the strength drops to the same level as that of the loosely packed material. In effect, the densely packed grains have been converted into the dilatent state.

Osborne Reynolds (1885) described this phenomenon long ago, and it is presently a staple of texts on soil mechanics [*Lambe and Whitman*, 1979].

The implication of this modification is that G in Equation 5 must be replaced by ρc_s^2 , where c_s is the effective shear wave speed in the dilatent material. This “effective” speed probably does not correspond to the propagation of any actual waves, but is a quantity defined by the equation $c_s = \sqrt{G/\rho}$, similar to the way the friction velocity is defined from the bed shear stress in sediment transport theory [*Bagnold*, 1966]. We derive an estimate of 2 MPa for the shear modulus in a medium sub-angular sand from a graph of deviator stress versus axial strain data recorded during a triaxial test [Fig. 12.9 in *Lambe and Whitman*, 1979, p. 159]. Using this value for G and a density of 2000 kg m⁻³ for the mass of granular debris, we find that the effective shear wave speed c_s is approximately 30 ms⁻¹.

Inserting this modification into the derivation of the relationship between the driving stress τ and strain rate $\dot{\epsilon}$ for a volume of acoustically fluidized debris, gives:

$$\dot{\epsilon} \approx \frac{\tau \nu}{\rho \lambda c_p} \left[\frac{1 - \text{erf}(\chi)}{1 + \text{erf}(\chi)} \right], \quad (6)$$

assuming that the pressure fluctuations follow a gaussian amplitude-frequency distribution [*Melosh*, 1979]. In this equation, ρ is the bulk density of the granular debris, $\nu = (c_p/c_s)^2$ is the square of the compressional-wave velocity c_p divided by the shear-wave velocity c_s , λ is the wavelength of the acoustic vibrations, and

$$\chi = \frac{p - \tau/\mu}{2c_p \sqrt{\rho E}}, \quad (7)$$

where p is the overburden pressure and E is the acoustic energy (energy in elastic waves) per unit volume.

A comparison between Equation 6 and the flow law for a Newtonian fluid ($\tau = 2\eta\dot{\epsilon}$), defines an effective Newtonian viscosity for the fluidized debris:

$$\eta_{\text{eff}} \approx \frac{\rho \lambda c_p}{2\nu} \left[\frac{2}{\text{erfc}(\chi)} - 1 \right]. \quad (8)$$

The function in the square brackets in Equation 8 is, effectively, a switch, controlled most crucially by the acoustic energy density. For a large enough acoustic energy density, the function in the square brackets is close to unity; thus, the effective viscosity is low (of the order $\rho \lambda c_s^2/c_p$) and the strain rate is large. For low acoustic energy densities, however, the function in the square brackets, and hence the effective viscosity of the fluidized debris, becomes very large. In such situations the strain rate of the debris is extremely small. Examining the viability of the acoustic fluidization model for the mobility of dry rock avalanches, therefore, requires an understanding of the temporal and spatial evolution of the acoustic energy within a granular medium.

2.3. Describing the temporal and spatial behavior of acoustic energy

To apply the theory of acoustic fluidization to a moving volume of rock debris, a rationale for describing the space- and time-dependent behavior of the acoustic energy must be developed. Here we assume that the short-wavelength elastic wave propagation is dominated by scattering. In this case, the most useful descriptor of the wave energy is

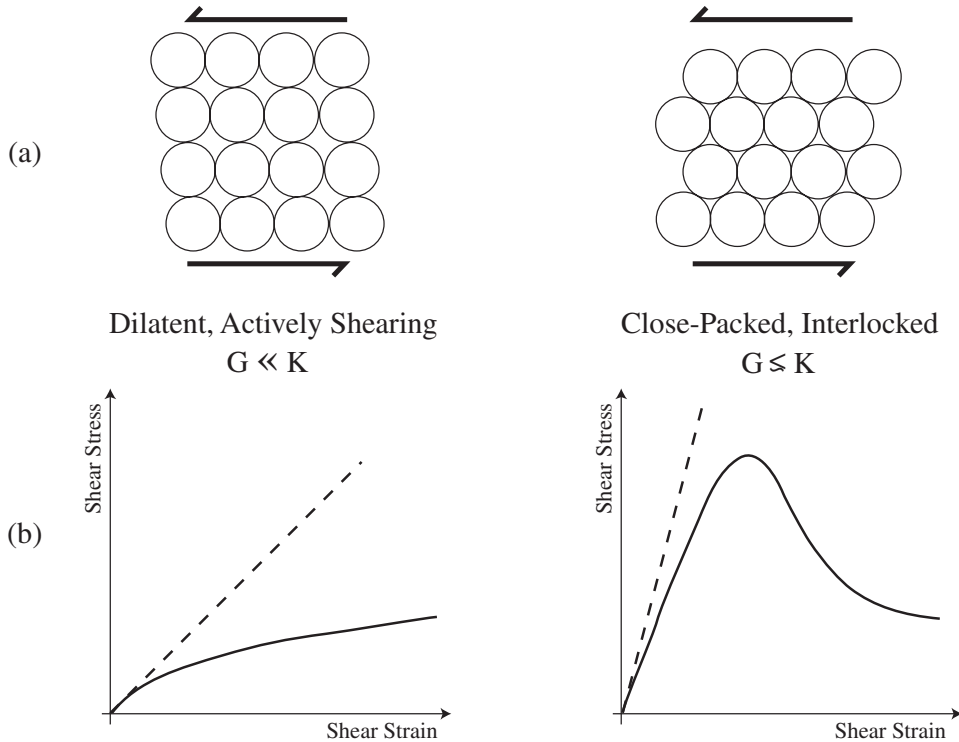


Figure 3. (a) Schematic illustration of the difference between actively shearing, dilatant materials and close-packed, dense granular materials. (b) Schematic stress/strain curves illustrating the difference in behavior of these two granular states.

the elastic energy density E , whose propagation can be described by a diffusion equation [Dainty and Toksöv, 1977]. This approximation is best thought of as an end member of a spectrum of elastic energy propagation modes. At the scattering end, the propagation of an elastic wave is strongly disrupted by heterogeneities in the acoustic properties of a material. The elastic waves undergo multiple diffractions and mode conversions (from compressional waves to shear waves or vice-versa) and a random wave-field develops behind the initial signal. Hence, the wave energy diffuses through the medium much slower than the sound speed. At the other end of this spectrum is Brune’s normal fluctuation model [Brune *et al.*, 1993], where normal stresses are excited by a wave coherent with the slip phase. In this case, any heterogeneities in the acoustic properties of the material are on a small enough scale that they do not impede the propagation of the elastic wave, and the energy in the wave is transported at the compressional wave speed for the material. In the case of the motion of shattered rock debris, the short wavelengths of the vibrations make strong scattering likely. Furthermore, recent work has shown that a substantial amount of energy is scattered into the coda of even normal seismic waves. The energy decline in these codas is also well described by a diffusion-type equation [Frankel and Wennerberg, 1987]. However, for acoustic vibration wavelengths of the order of the avalanche thickness, the scattering approximation becomes invalid.

The energy balance of short-wavelength vibrations within a granular medium may be formally derived by considering a control volume within the avalanche, which is small compared to the thickness of the avalanche, but large compared to the wavelength. Elastic wave energy can be scattered into or out of the volume. Once inside, it can be absorbed as heat, or it can facilitate the movement of the slide and generate new elastic energy. The full equation governing these possibilities is:

$$\frac{dE}{dt} = \frac{\xi}{4} \nabla^2 E - \frac{c_p}{\lambda Q} E + e \tau_{ij} \dot{\epsilon}_{ij}, \quad (9)$$

[Melosh, 1996]. The left-hand side of the equation describes the rate of change of the elastic energy density E in the control volume, with respect to time. Strictly speaking, as the control volume is fixed in space, the derivative is a convective material derivative and should be written in full as $dE/dt + v_i \nabla_i E$, where v_i is the velocity vector for material moving through the control volume. However, by assuming the avalanche is infinitely long and, thus, that the downslope velocity gradient is zero, this distinction can be ignored.

The first term on the right-hand side is the scattering term, where ξ is the scattering diffusivity, which has dimensions of a length times a velocity. The second term parameterizes conversion of elastic energy into heat. Q is defined as the ratio of the energy stored per cycle to the energy dissipated in the same period. The last term quantifies the rate of acoustic energy generation during flow. The product of the space and time average of stress and strain rate tensors, $\tau_{ij} \dot{\epsilon}_{ij}$, gives the total rate of energy dissipation for the control volume, which is multiplied by an efficiency parameter e ($0 < e < 1$) to give the rate of energy dissipated in the form of acoustic vibrations. It is this positive-feedback term that leads to interesting behavior—an important aspect of the acoustic fluidization model is that energy dissipated by shear in the flowing debris can itself generate acoustic energy. In static regions the vibrations might dissipate quickly by friction and the effective viscosity in those regions would rapidly rise; however, in flowing regions the regeneration of acoustic energy could permit flow to continue until the driving stresses are relieved.

3. Steady-state solution for an acoustically fluidized rock avalanche

Equation 9 is a nonlinear partial differential equation that depends on three spatial variables and time. Solving this equation numerically is extremely complicated without invoking some simplifying assumptions. To test the acoustic fluidization hypothesis for the mobility of large rock avalanches, we are interested in the spatial and temporal development of the acoustic energy field within the avalanche. In particular, we wish to know: (1) whether there is a steady-state solution to the acoustic energy balance equation that predicts self-sustaining flow of the avalanche; and (2) if such a solution exists, whether it may be obtained from realistic initial conditions. Thus, before discussing time-dependent solutions, it is insightful to seek steady-state solutions for a wide-sheet avalanche, moving down a slope of constant angle.

3.1. Method

For a steady-state solution, that is, a solution that does not change with time, the left-hand side of Equation 9 is zero ($dE/dt = 0$). Furthermore, as the avalanche is assumed to be infinitely wide and long, all spatial derivatives in the direction of the avalanche plane also vanish. If z is the distance from the top of the avalanche, measured normal to the plane of the avalanche, then the only non-zero derivatives are with respect to z , and the only non-zero component of the strain rate tensor is $\dot{\epsilon}_{zx}$. In this case, Equation 9 simplifies to:

$$\frac{d^2 E}{dz^2} = \frac{4}{\xi} \left(\frac{c_p}{\lambda Q} E - 2e\tau_{zx}\dot{\epsilon}_{zx} \right), \quad (10)$$

which may be written in full by substituting Equation 6 for the average strain rate $\dot{\epsilon}_{zx}$ of a granular material in the presence of acoustic pressure vibrations and Equation 4 for the shear stress within the avalanche τ_{zx} . This gives:

$$\frac{d^2 E}{dz^2} = \frac{4c_p}{\xi\lambda Q} \left(E - 2e\nu Q \sin^2 \theta \frac{(\rho g z)^2}{\rho c_p^2} \Phi \right), \quad (11)$$

where Φ is given by:

$$\Phi = \left[\frac{1 - \operatorname{erf}(\chi)}{1 + \operatorname{erf}(\chi)} \right]; \quad (12)$$

in which χ (given by Eq. 7) is defined as:

$$\chi = \frac{\rho g z \left(\cos \theta - \frac{\sin \theta}{\mu} \right)}{2c_p \sqrt{\rho E}}. \quad (13)$$

Analysis of this equation can be simplified by normalizing the various terms by constant quantities of the same dimensions and some convenient size. Thus, the acoustic energy density E is normalized by the acoustic energy density required to support the overburden pressure at the base of the avalanche, E_h :

$$\Psi = \frac{E}{E_h} = \frac{E}{\left[\frac{(\rho g h)^2}{\rho c_p^2} \right]}; \quad (14)$$

and distances z are normalized by the avalanche thickness h : $\zeta = z/h$, implying $\zeta = 0$ at the top of the avalanche and $\zeta = 1$ at the base. In terms of these non-dimensional variables the combination of Equations 11–13 simplify to:

$$\frac{d^2 \Psi}{d\zeta^2} = \frac{1}{\gamma^2} \left[\Psi - r\zeta^2 \left(\frac{1 - \operatorname{erf}\left(\frac{\alpha\zeta}{\sqrt{\Psi}}\right)}{1 + \operatorname{erf}\left(\frac{\alpha\zeta}{\sqrt{\Psi}}\right)} \right) \right]. \quad (15)$$

In this equation, α is a dimensionless measure of the stability of the avalanche, given by:

$$\alpha = \frac{1}{2} \left(\cos \theta - \frac{\sin \theta}{\mu} \right); \quad (16)$$

which varies from $\alpha = 0.5$, for a slope angle of zero, to $\alpha = 0$, for a slope angle equal to the maximum angle of stability ($\theta = \theta_m = \tan^{-1} \mu$). It may appear from Equation 16 that α can be negative if the slope angle exceeds the maximum angle of stability; however, in this case the equations discussed here do not apply—acoustic fluidization is not required to mobilize the debris.

The parameter r quantifies the amount of energy available for regeneration, given by:

$$r = 2e\nu Q \sin^2 \theta. \quad (17)$$

The minimum value of r is zero, which corresponds to situations where no energy is regenerated.

Finally, γ is a dimensionless measure of the amount of scattering, defined as the scattering length l_* (the distance over which the acoustic energy density falls by a factor of e) divided by the avalanche thickness h :

$$\gamma = \frac{l_*}{h} = \frac{1}{h} \sqrt{\frac{\xi\lambda Q}{4c_p}}. \quad (18)$$

The smaller γ is, the greater the effect of scattering; that is, the shorter the distance acoustic energy may propagate in a given time.

Equation 15 describes how the acoustic energy must vary with vertical position within the avalanche for the acoustic energy field to be stable in time. Solutions to this equation, therefore, define vertical profiles of acoustic energy versus depth in the rock avalanche. The character of these solutions is entirely controlled by the three parameters α , r and γ , and the boundary conditions. We assume that at the top of the avalanche free slip is permitted, while at the base of the avalanche there is a no-slip condition. The base of the slide defines the interface between the moving avalanche and the sloping solid ground beneath. Acoustic energy is transmitted across this boundary. However, the lack of motion ($\dot{\epsilon}_{zx} = 0$) within the ground implies that no regeneration occurs in the ground beneath the slide. We assume that γ is the same in both the flowing avalanche and the stationary ground beneath, but this is not essential.

If there is no regeneration of acoustic energy within the avalanche then the solution to Equation 15 is trivial: $\Psi = 0$ everywhere. However, if the avalanche is generating acoustic energy, then the solution to Equation 15 within the ground beneath the avalanche, where the absence of motion implies $r = 0$, will be of the form: $\Psi = ae^{b\zeta}$. Substituting this and $r = 0$ into Equation 15 gives $b = \pm 1/\gamma$, and, assuming that the acoustic energy at base of the moving avalanche is fixed ($\Psi = \Psi_h$ at $\zeta = 1$), then $a = \Psi_h e^{\mp 1/\gamma}$. Thus, the only sensible solution to Equation 15 in the ground beneath the avalanche is:

$$\Psi = \Psi_h e^{\frac{1-\zeta}{\gamma}}, \quad (\zeta \geq 1). \quad (19)$$

If there is strong scattering of acoustic energy within the avalanche; that is, $\gamma \approx 0$, then the solution to Equation 15 is straightforward:

$$\Psi = r\zeta^2 \left(\frac{1 - \operatorname{erf}\left(\frac{\alpha\zeta}{\sqrt{\Psi}}\right)}{1 + \operatorname{erf}\left(\frac{\alpha\zeta}{\sqrt{\Psi}}\right)} \right) \sim r\zeta^2. \quad (20)$$

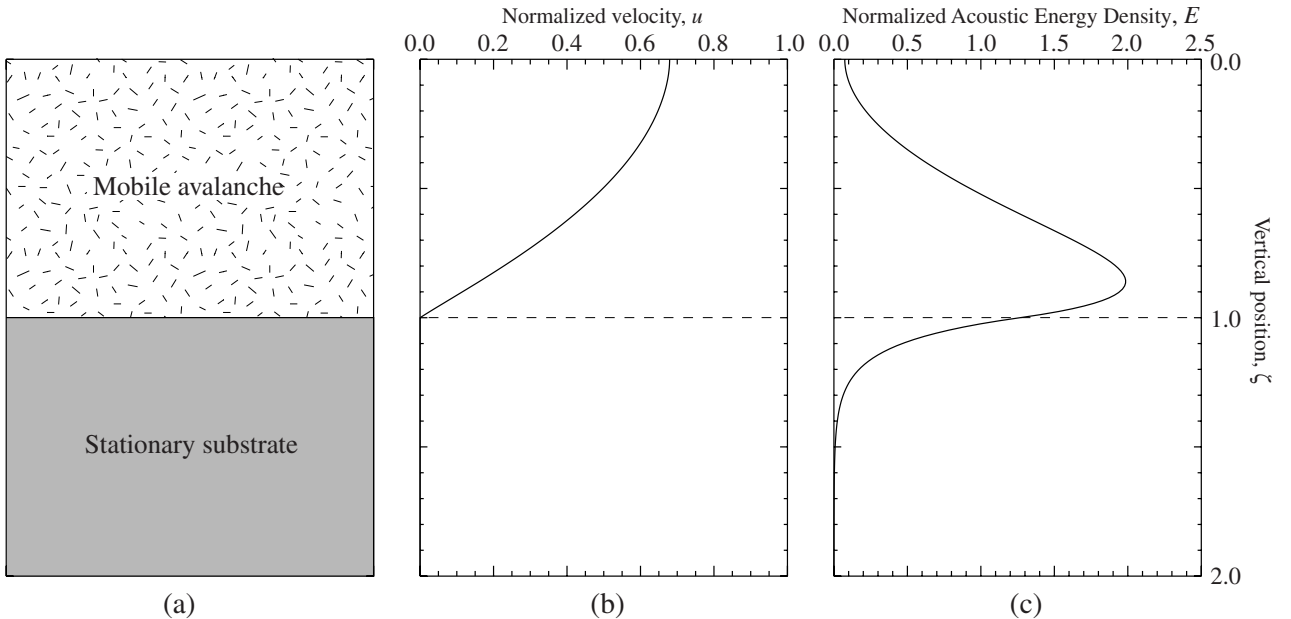


Figure 4. An example of one solution to Equation 15, for $r = 5.0$, $\gamma = 0.1$, $\alpha = 0.32$, with a reflective acoustic energy boundary at the surface ($dE/dt(\zeta = 0) = 0$). The left panel (a) depicts the modeled situation of a mobile rock avalanche moving over a stationary substrate. The center panel (b) illustrates the velocity profile through the flowing avalanche. The right panel (c) shows the acoustic energy profile.

Thus, if the regeneration parameter r is non-zero, the acoustic energy density is proportional to the square of the distance from the top of the slide and the argument of the error function χ is approximately constant. Substituting this result ($\chi = \text{constant}$) into Equation 8 illustrates that, in cases of strong scattering, the effective viscosity of the fluidized avalanche should be independent of depth. This implies that the velocity profile through the avalanche should be parabolic and not a narrow shear-zone at the base of the slide with a steep velocity gradient.

For a more general set of steady-state solutions to the acoustic energy balance equation, we integrate Equation 15 using a fourth-order Runge-Kutta integrator and a bisectational shooting method that starts with an assumed energy density at the base of the slide $\Psi(\zeta = 1)$, then integrates upward into the avalanche, and downward into the ground. Two solutions are sought: one for which $d\Psi/d\zeta = 0$ at $\zeta = 0$, which assumes that the top of the slide acts as a reflective boundary to acoustic energy; and one for which $\Psi(0) = 0$, which assumes that the acoustic energy density at the surface is zero. These two solutions may be thought of as end-member cases where either no acoustic energy leaks out from the free surface, or all acoustic energy near the top of the avalanche is lost through the free surface.

In the ground beneath the slide ($\zeta > 1$) the rock is assumed to be cohesive; thus, the strain rate $\dot{\epsilon} = 0$, for $\zeta > 1$, and no elastic energy regeneration occurs. However, because acoustic energy can scatter into the ground beneath the slide, the acoustic energy density declines exponentially to zero with increasing depth beneath the slide, as stated in Equation 19.

When a solution is found for the energy density, the non-dimensional velocity of the flow in the direction parallel to the plane of the slide u can be determined from the strain rate. In terms of the non-dimensional parameters used in

Equation 15, the equation for the strain rate of acoustically fluidized debris (Eq. 6) may be written as:

$$\dot{\epsilon} = \frac{\nu gh \sin \theta}{\lambda c_p} \zeta \left(\frac{1 - \text{erf}\left(\frac{\alpha \zeta}{\sqrt{\Psi}}\right)}{1 + \text{erf}\left(\frac{\alpha \zeta}{\sqrt{\Psi}}\right)} \right). \quad (21)$$

Thus, by recalling that $\dot{\epsilon}_{zx} = 0.5(dv_x/dz)$, where x is the direction of slip and by defining the non-dimensional, downslope avalanche velocity u as:

$$u = \frac{\lambda c_p}{\nu gh^2 \sin \theta} v_x, \quad (22)$$

the normalized downslope velocity, as a function of depth within the avalanche, may be determined by numerical integrating:

$$\frac{du}{d\zeta} = 2\zeta \left(\frac{1 - \text{erf}\left(\frac{\alpha \zeta}{\sqrt{\Psi}}\right)}{1 + \text{erf}\left(\frac{\alpha \zeta}{\sqrt{\Psi}}\right)} \right). \quad (23)$$

3.2. Results

An example of one steady-state solution to the acoustic fluidization equations for a dry rock avalanche is shown in Figure 4. Figure 4a depicts the modeled situation of a mobile rock avalanche moving over a stationary substrate. The velocity profile through the flowing avalanche is almost parabolic, rising from zero at the base of the slide to a maximum at the free surface (Figure 4b). The acoustic energy is concentrated near the base of the slide and drops to zero at the top of the slide and beneath the base of the slide (Figure 4c). The drop in acoustic energy density beneath the slide is much more abrupt than the drop within the avalanche, and is due to the absence of regeneration of acoustic energy in the ground. The drop in acoustic energy towards the top of the slide is due to the reduction in shear stress towards the top of the slide and, consequently, the amount of acoustic energy regenerated. The fact that

the velocity profile of the slide is almost parabolic, as would be expected for a constant viscosity fluid, implies that the acoustically fluidized avalanche generates a natural balance between the increasing overburden pressure and the increasing acoustic energy density with depth.

The maximum flow velocity in Figure 4b is approximately 0.7. For a 10-metre thick avalanche on a 10 degree slope on Earth, with a compressional wave velocity of 100 ms^{-1} , a shear wave velocity of 30 ms^{-1} ($\nu \approx 10$), and an acoustic vibration wavelength of 0.1 m, this would correspond to an avalanche speed of roughly 100 ms^{-1} , which is in accordance with estimated velocities of sturzstroms [Shaller, 1991, and references therein]. Larger, thicker avalanches will travel faster.

Non-linear partial differential equations, like the energy balance equation (15), often have solutions for only a limited range of the controlling parameters. The region of the parameter space for which solutions exist represents the conditions under which the process being modeled may operate. Figure 5 illustrates those values of γ and r for which solutions to Equation 15 exist, for various values of the slope stability parameter α . The solid line in Figure 5 represents the solution boundary in r - γ space, for a slope angle of approximately 10° . For all combinations of r and γ that lie above this line, there exists a solution to the acoustic energy balance equation, of a form similar to that illustrated in Figure 4. Thus, for that particular set of parameters, r , γ and α , acoustic fluidization facilitates self-sustaining downslope flow of the rock avalanche. In other words, the acoustic energy generated by the motion of the rock avalanche is sufficient to balance the acoustic energy losses due to dissipation and scattering; hence, a stable acoustic energy field develops within the avalanche. For all points below the line, however, no solution exists, indicating that acoustic fluidization cannot sustain steady motion of the avalanche, for those combinations of r , γ and α . Under these circumstances, acoustic energy losses by dissipation and scattering outweigh the generation of acoustic energy due to the motion of the avalanche; hence, the acoustic energy field decays away and

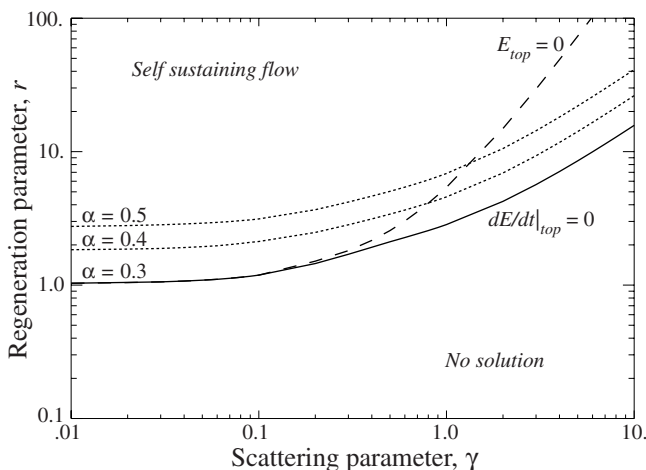


Figure 5. Plot illustrating the parameter space for which steady-state solutions exist to the acoustic energy balance equation, for a wide-sheet avalanche traveling down a constant slope. Shown are the solution boundaries in r - γ space, for various different values of slope stability, α ; and for the two top boundary conditions. See text for further details.

the rock avalanche loses its mobility. The dotted lines show that a larger regeneration parameter is required to facilitate self-sustaining flow of the avalanche as the slope stability parameter increases; that is, as the slope angle decreases.

Also shown in Figure 5 is the effect of the different boundary conditions: the solid line illustrates the reflective top boundary case ($dE/dt(0) = 0$) and the dashed line illustrates the case where there is no acoustic energy at the surface ($E(0) = 0$). The difference between the two curves is negligible for values of γ less than about 0.1. For values of γ in excess of this, the $E(0) = 0$ boundary condition is more restrictive than the $dE/dt(0) = 0$ condition; that is, a greater amount of regenerated acoustic energy is required, for a given value of γ , to sustain flow in the case of zero acoustic energy density at the top of the avalanche, than that required when there is a reflective boundary condition at the free surface.

3.3. Implications

Our steady-state analysis shows that acoustic fluidization can theoretically sustain fluid-like motion of a dry rock avalanche for certain combinations of the controlling parameters. Whether or not this process is important for real rock avalanches, therefore, hinges on knowledge of these parameters for a typical rock avalanche. Unfortunately, several of the acoustic fluidization model parameters are not yet constrained by observation. For example, the scattering diffusivity ξ is completely unconstrained. The dominant wavelength of the acoustic vibrations λ has not been measured directly. However, to be consistent with the acoustic fluidization theory, it must be much smaller than the thickness of the avalanche (typically tens to hundreds of meters for sturzstroms) and much larger than the minimum grain size (\sim mm), giving an approximate range of 1 cm–1 m. The dissipation quality factor Q as defined here has also not been measured directly. A similar quantity, the seismic Q has been measured to be around 500 for the crust and upper mantle. However, this value includes both loss by conversion to heat and loss by scattering, and is therefore likely to be a lower estimate for the Q defined here, which does not count scattering as a loss. Thus, the only constraint that can be placed on the scattering parameter γ is that it is unlikely to exceed 10. Figure 5 illustrates that, for stable, steady-state solutions to the acoustic fluidization equation for a dry rock avalanche to exist, the regeneration parameter ($r = 2e\nu Q \sin^2 \theta$) must be ≥ 1 if $\gamma < 1$. Hence, for a dissipation quality factor $Q \sim 500$ (comparable to the seismic Q in the upper crust), $\nu \approx 10$, and a slope angle of 2° , the required efficiency for converting elastic strain energy into elastic-wave energy, e , is about 0.1, which is well below typical estimates of around 0.5 [Kanamori, 1994]. Therefore, although there are large uncertainties in the model parameters, sensible estimates suggest that acoustic fluidization can realistically facilitate self-sustaining motion of a sufficiently large dry rock avalanche.

The steady-state solutions to the acoustic fluidization equations for a dry rock avalanche all suggest that the sturzstrom flows with a viscosity that is almost independent of depth. Observations of a viscous fluid traveling downslope show that the front lobe becomes extremely distorted with fluid at the top of the lobe rolling down the front of the lobe and then being dragged underneath the advancing fluid, in analogy with caterpillar tracks on all-terrain

vehicles. Thus, it may seem difficult to reconcile constant viscosity flow of the avalanche with the common observation of gross stratigraphy preservation during a large avalanche event [for example *Shreve*, 1968]. However, discrete-element computer simulations of large rock avalanches by *Campbell et al.* [1995], involving thousands to millions of particles, show both constant-viscosity flow (parabolic velocity profile) within the bulk of the avalanche and stratigraphy preservation. The important proviso to the constant viscosity flow model might be that the front lobe of the avalanche is not fluidized and operates as a rigid plug that retards deformation of the avalanche-front, while allowing the bulk of the avalanche to flow with a more uniform viscosity.

The shape of the solution boundaries depicted in Figure 5 provides a potential explanation for the volume-mobility relationship for large rock avalanches. Recall that γ is the ratio of the acoustic energy scattering length to the thickness of the avalanche. This implies that moving from left to right along the horizontal axis in Figure 5 corresponds to either an increase in the scattering length, or a decrease in the landslide thickness. If we assume that the regeneration parameter and the scattering length are constant for all rock avalanches, regardless of volume, then, provided the regeneration parameter is large enough, there exists a minimum avalanche thickness above which acoustic fluidization may enable self-sustaining fluid-like flow of the rock avalanche at low slope angles. For an avalanche thickness lower than this critical limit, the effect of acoustic fluidization would be insufficient to sustain motion of the avalanche. In such cases, the movement of the avalanche would be instead controlled by standard debris mechanics; flow would occur only if the slope angle exceeds the maximum angle of stability. The termination of an avalanche might, therefore, correspond to the moment when the avalanche has thinned to this critical avalanche thickness. Thus, the greater the original thickness of the avalanche, and hence the volume of debris involved, the further the avalanche may travel before the critical thickness is reached. Scatter in the exact value of this thickness would arise from differing slope angles and slight differences in the regeneration parameter and scattering length between different avalanches.

Using the logic just described, a quantitative prediction of the relationship between the ratio H/L and avalanche volume for an acoustically mobilized sturzstrom may be derived from a simple volume conservation argument. Consider the idealized schematic of the emplacement of a large rock avalanche illustrated in Figure 6, where the rock mass falls a distance H before running out almost horizontally a distance of L . After the initial fall of distance H , it may be assumed that the avalanche occupies an area A_0 , approximately equal to square of the fall height $A_0 \approx H^2$. Thus, if the initial (post-fall, pre-runout) avalanche thickness is h_0 , the volume of the rock avalanche is given as $V \approx h_0 H^2$. When runout is complete and the avalanche has come to rest, its final areal extent will be on the order of L^2 ; hence, the final volume of the rock avalanche is given by $V \approx h_f L^2$, where h_f is the final thickness of the avalanche. By equating these two volumes and rearranging we find that the effective coefficient of friction, $H/L \approx \sqrt{h_f/h_0}$. Thus, if h_f represents the critical avalanche thickness below which acoustic fluidization cannot mobilize the rock mass and which is approximately constant for all avalanches, the effective coefficient of friction will be approximately proportional to one over the square root of the initial avalanche thickness ($H/L \propto h_0^{-1/2}$). We find that this is in close agreement with the observed trend of effective coefficient of friction versus avalanche volume, if the

initial avalanche thickness is proportional to the cube root of the avalanche volume ($h_0 \propto V^{1/3}$). In this case, the effective coefficient would scale with the avalanche volume to the negative one-sixth power ($H/L \propto V^{-1/6}$), which is remarkably similar to the relationship suggested by the slope of the best fit lines for the terrestrial and Martian data points in Figure 1 ($H/L \propto V^{-0.16}$).

As discussed earlier, the phenomenological models of *Dade and Huppert* [1998] and *McEwen* [1989] suggest that the volume-mobility relationship for large rock avalanches can be explained by a constant stress resistance of 10-100 kPa. This corresponds to the normal stress associated with 1 – 10 meters of overburden on Earth. Using this as a range for the critical avalanche thickness below which acoustic fluidization cannot mobilize the avalanche, we can place limits on the most unconstrained parameter in our study, the scattering diffusivity ξ . If, during the emplacement of a sturzstrom, the thickness of the acoustically fluidized avalanche gradually drops until it reaches the critical thickness ($h_f \sim 1 - 10$ m), this corresponds to moving horizontally across Figure 5 until γ is greater than about 1.0. If we assume that $\gamma \sim 1$ is the critical point above which acoustic fluidization cannot mobilize the avalanche, and that the acoustic wavelength scales as some small fraction β of the avalanche thickness, then substitution into Equation 18 gives:

$$\xi \approx \frac{4c_p h_f}{\beta Q}. \quad (24)$$

Thus, for $h_f = 1 - 10$ m, $c_p = 100$ ms⁻¹, $Q = 500$ and $\beta = 0.1$ we learn that $\xi \approx 10-100$ m²s⁻¹.

4. Time-dependent solutions

4.1. Method

To test the stability of the steady-state solutions discussed above, and to investigate the effect of initial conditions on the solution, we have extended the numerical treatment described above to include time-dependency. We achieve this using a computational tool for studying fluid flow: a hydrocode. The hydrocode used is SALES 2, a multi-material hydrocode with a Coulomb-elastic-plastic strength model, based on the SALE hydrocode [*Amsden et al.*, 1980]. We use the hydrocode in a purely Eulerian mode: the computational mesh is fixed; it encompasses a region of the sloping ground and a region above it through which the rock

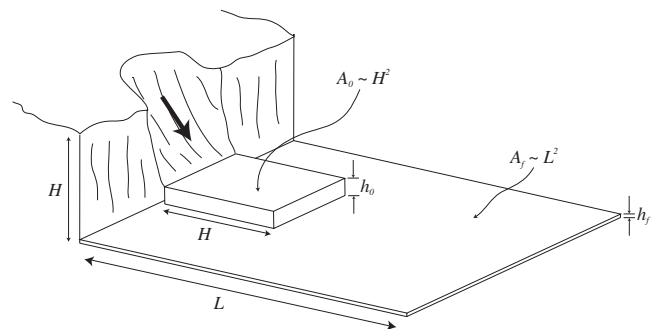


Figure 6. Schematic illustration of a rock avalanche emplacement. After an initial fall of height H , the rock avalanche occupies a region approximately H by H by h_0 ; after runout the avalanche occupies a region L by L by h_f . See text for further details.

avalanche passes. To avoid problems associated with tracking the free surface within the mesh, we define the top of the mesh to be the free surface. This requires that the thickness of the avalanche remain constant. Thus, an implicit assumption in our modeling work is that the avalanche is infinitely long, and that material enters one side of the mesh at the same rate as material leaves the opposite side; that is, no pressure gradient exists in the direction of flow.

In the absence of acoustic energy, the strength of the rock avalanche is defined by Coulomb friction (Equation 1). The ground beneath is assumed to obey a similar strength law, modified to include a cohesion, which defines the ground as intact rock. For stresses below this shear strength, the mass of granular debris is modeled as an elastic solid; when the driving stress exceeds the shear strength the granular debris is modeled as a Newtonian fluid.

The effect of slope angle is introduced by modifying the horizontal and vertical components of gravity imposed on the mesh. To confirm that the behavior of the modeled situation agrees with the mechanics of granular debris, we conducted some preliminary calculations: the horizontal and vertical gravity components were altered to simulate slowly increasing the slope angle until flow in the debris was initiated. Reassuringly, the corresponding slope angle was found to be the cotangent of the prescribed coefficient of friction, as predicted by Coulomb's law.

To incorporate the effects of acoustic fluidization, we modified SALES 2 to include a new scalar, cell-centered parameter, the acoustic energy per unit mass. This *specific* acoustic energy \mathcal{E} is related to the acoustic energy density E by:

$$\mathcal{E} = \frac{E}{\rho}. \quad (25)$$

To simulate the spatial and temporal evolution of the specific acoustic energy, as influenced by the effects of scattering, dissipation and regeneration, we implemented a modified version of the acoustic energy balance equation (Eq. 9) in SALES 2. At every time-step the new specific acoustic energy in each cell \mathcal{E}_n is updated from the existing specific acoustic energy \mathcal{E}_{n-1} (where the subscript denotes the time-step number) using the equation:

$$\mathcal{E}_n = \mathcal{E}_{n-1} + \mathcal{E}_s + \mathcal{E}_d + \mathcal{E}_r \quad (26)$$

where \mathcal{E}_s , \mathcal{E}_d , \mathcal{E}_r are the changes in specific acoustic energy due to the effect of scattering, dissipation and regeneration, respectively.

The change in specific acoustic energy in one time-step (interval of dt seconds) due to scattering, is calculated on a cell-by-cell basis using:

$$\mathcal{E}_s = \frac{\xi}{4} \left(\frac{d^2 \mathcal{E}}{dx^2} + \frac{d^2 \mathcal{E}}{dz^2} \right) dt, \quad (27)$$

where ξ is an input parameter. Note that, because the avalanche simulations are two-dimensional, the scattering in the y -direction is assumed to cancel out.

The change in specific acoustic energy due to dissipation of acoustic energy as heat, is calculated for each cell using:

$$\mathcal{E}_d = -\frac{c_p}{\lambda Q} \mathcal{E}_{n-1} dt, \quad (28)$$

where c_p , λ and Q are all input parameters.

Finally, the amount of specific acoustic energy regenerated per time-step is calculated for each cell using:

$$\mathcal{E}_r = \frac{e}{\rho} \Pi_{ij} \dot{\epsilon}_{ij} dt, \quad (29)$$

where e is an input parameter and ρ is the density of the rock debris in the cell. Π_{ij} and $\dot{\epsilon}_{ij}$ are the deviatoric stress and strain rate tensors for the cell, respectively; summation over the indices is implied.

As discussed above, the presence of acoustic energy within a mass of rock debris changes the rheology of the debris to that of a fluid. In our modeling, we simulate this by defining an effective viscosity for each cell using Equation 8, where the argument of the complementary error function χ , in terms of the specific acoustic energy, is:

$$\chi = \frac{p - \tau/\mu}{2\rho c_p \sqrt{\mathcal{E}}}. \quad (30)$$

In this equation p is the pressure in the cell, ρ is the density of the rock debris in the cell and τ is the maximum shear stress in the cell; μ and c_p are input parameters.

The modifications described above allow SALES 2 to simulate the behavior of an acoustically fluidized rock avalanche. First, a mesh is generated to represent the avalanche and within this an initial acoustic energy field or velocity field is defined. This acoustic energy field affects the rheology of the rock avalanche; the greater the amount of acoustic energy in a cell, the lower the effective viscosity and, hence, the lower the resistance to flow. As time progresses, the acoustic energy field in the mesh changes due to scattering, dissipation, and, as the avalanche begins to move, regeneration of acoustic energy. The key question to be answered with this tool is then: under what conditions can the motion of the acoustically fluidized rock avalanche reach a stable steady-state?

4.2. Results

We performed hundreds of hydrocode simulations to explore the effects of the various input parameters. Table 1 describes the input parameters for the hydrocode simulation and defines values, or ranges of values, used in our investigation of their effects. In the interest of brevity we discuss only the most important relationships.

To first compare results from our hydrocode simulations with the steady-state solutions discussed in the previous section, we performed several simulations in which the initial acoustic energy field was equal to E_h everywhere in the avalanche. In other words, the normalized specific acoustic energy at time $t = 0$, Ψ_0 , was set equal to 1.0 in every cell within the avalanche. For these simulations we used various combinations of input parameters that gave the same set of values for r , γ and α , for which a steady-state solution was known to exist. We found that in all cases the hydrocode simulation results were in excellent agreement with the steady-state solution. During the simulations, the avalanche eventually reached a state where there was a stable acoustic energy field within the avalanche, allowing the avalanche to maintain mobility and travel at a constant velocity. Furthermore, the final form of the acoustic energy field and velocity profile was identical to that predicted by the steady-state analysis; that is, of the form shown in Figure 4.

The next stage in our investigation was to compare the region of input-parameter space for which stable hydrocode simulation results were achieved, with the region of r - γ space for which steady-state solutions exist (as shown in Figure 5). Figure 7 illustrates results from some of these simulations;

Table 1. Model parameters

Parameter	Symbol	Value
Density of rock debris avalanche	ρ	2000 kg m ⁻³
Compressional-wave speed for the rock avalanche	c_p	100 ms ⁻¹
Shear-wave speed for the rock avalanche	c_s	30 ms ⁻¹
Coefficient of internal friction	μ	0.5
Initial normalized specific acoustic energy	Ψ_0	0.01–100
Initial normalized avalanche velocity	u_0	0.0–2.0
Landslide thickness	h	8–128 m
Wavelength of acoustic vibrations	λ	0.04–2 m
Scattering diffusivity	ξ	0.64–32 m ² s ⁻¹
Regeneration efficiency parameter	e	0–1
Dissipation quality factor	Q	100–400
Slope angle	θ	1–30°

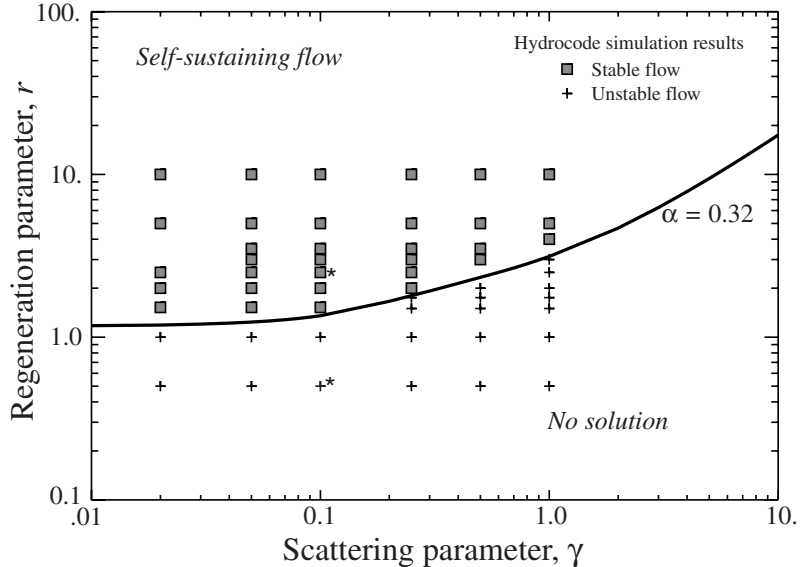


Figure 7. Region of parameter space for which stable and unstable time-dependent solutions for an acoustically fluidized rock avalanche exist, compared with the region of parameter space where steady-state solutions exist. The solid line represents the steady-state-solution boundary, in $r - \gamma$ space, for a slope angle of 10° and friction coefficient of 0.5 ($\alpha = 0.32$). The squares represent hydrocode simulations where a stable, steady solution developed. The crosses represent hydrocode simulations where the solution was unstable. The symbols with an adjacent star identify simulations discussed in further detail in the text and in Figure 8.

shown are results from simulations with a slope angle of 10° and friction coefficient of 0.5 ($\alpha = 0.32$). The squares represent hydrocode simulations where a stable, steady solution developed, describing the downslope flow of the rock avalanche. In such cases, the solution was identical to the corresponding steady-state solution. The crosses represent hydrocode simulations where the solution was unstable; that is, the effect of acoustic fluidization was insufficient to sustain downslope flow, and the motion of the avalanche ceased.

Figure 8 illustrates the difference between typical “stable” and “unstable” simulations. The two examples are marked with stars in Figure 7. The curves describe the development of the maximum avalanche velocity, and the maximum specific acoustic energy with time during the simulations. The solid curves, which are taken from a stable simulation, show that the avalanche reaches a state where there is a stable acoustic energy field within the avalanche, allowing the avalanche to travel at a constant velocity. The dashed curves, which are taken from an unstable calculation, show that in this case the acoustic energy field decays to zero, forcing the avalanche to stop.

Our hydrocode simulations begin with either an initial avalanche velocity or an initial acoustic energy field within the avalanche. We have investigated the effect of these initial conditions on the behavior of the simulated rock avalanche. Figure 9 illustrates the effect of various different initial avalanche velocities on the simulation results. The curves describe the development of the maximum avalanche velocity and the maximum specific acoustic energy in the avalanche with time, for five different simulations that differ only in the initial avalanche velocity. The solid curves represent simulations that result in a stable solution; that is, the avalanche achieves a stable velocity as a self-sustaining acoustic energy field develops in the avalanche. The dashed curves represent simulations where the acoustic energy field decays away and the avalanche comes to rest. Thus, for this particular suite of simulations, there is a critical value of the initial normalized avalanche velocity of about 0.1. For simulations with an initial normalized velocity greater than this value, the simulated rock avalanche achieves the same stable state.

For simulations that begin with an initial acoustic energy field within a stationary avalanche, a similar result is observed; that is, there is a critical magnitude for this initial

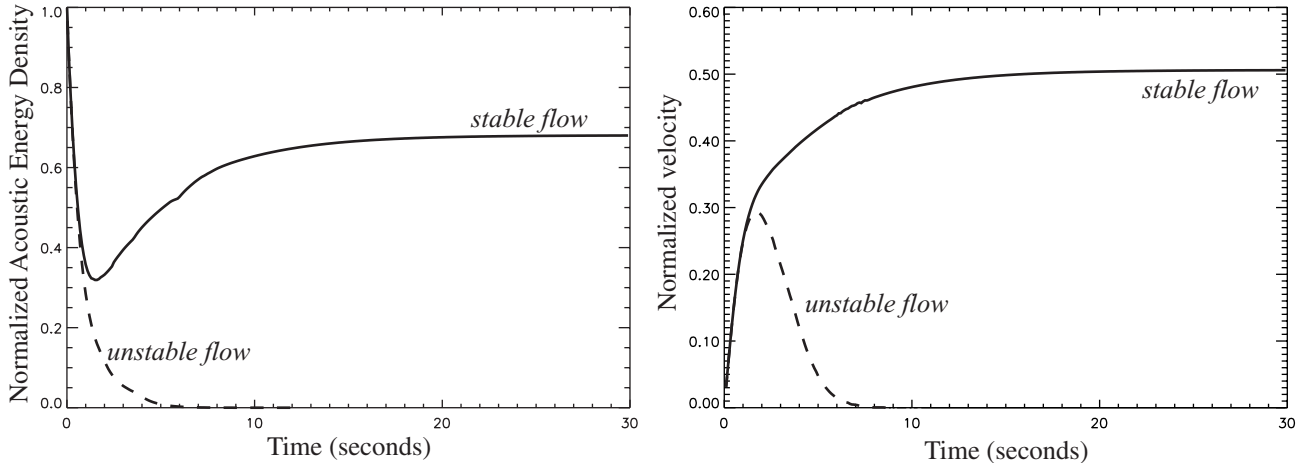


Figure 8. Plots illustrating the time-dependent behavior of the rock avalanche in our simulations. The left panel shows the change in maximum normalized acoustic energy density with time for two simulations. The right panel shows the development of the maximum avalanche velocity with time for the same two simulations. The solid curve represents a simulation during which the rock avalanche achieved a stable state (marked with a star in Fig. 7). The dashed curve represents a simulation where the acoustic energy decayed away and the avalanche came to rest (marked with a star in Fig. 7).

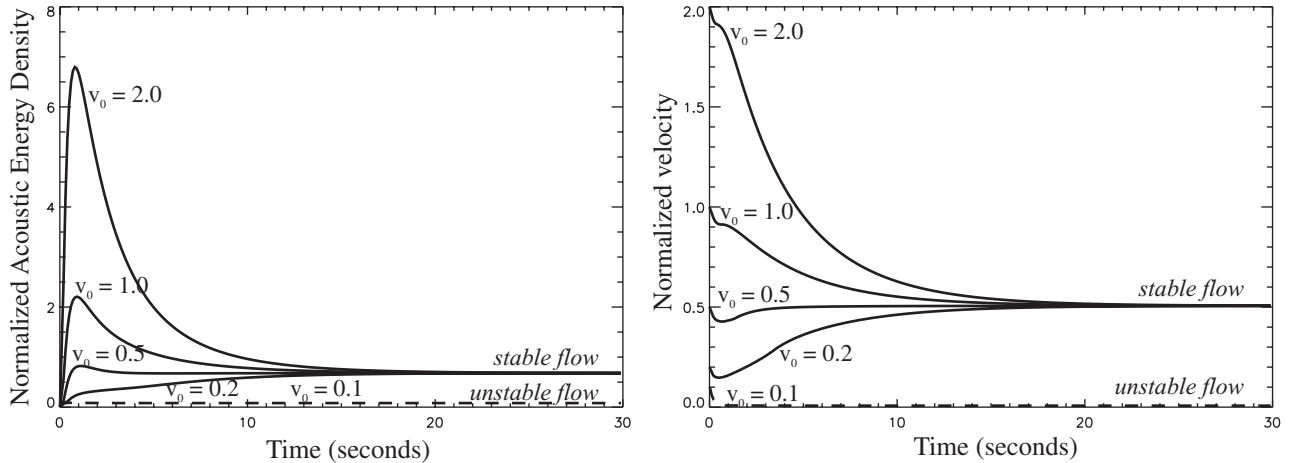


Figure 9. Plots illustrating the effect of initial conditions on our time-dependent simulations of an acoustically fluidized rock avalanche. The left panel shows the change in maximum normalized acoustic energy density with time for five simulations with different initial conditions. The right panel shows the development of the maximum avalanche velocity with time for the same five simulations. The five curves in each plot correspond to five different initial normalized avalanche velocities. The curves are all variations on the stable simulation marked with a star in Fig. 7.

acoustic energy field, above which the same self-sustaining acoustic energy field develops during the simulation. The critical values of these initial conditions depend upon other input parameters. For example, the critical initial avalanche velocity is less if the regeneration parameter r is large; that is, if the dissipation factor Q , the seismic efficiency e , or the slope angle θ are large. However, the critical normalized initial velocity of 0.1 is typical of the more restrictive limits.

4.3. Implications

The hydrocode simulation results are in remarkable agreement with the steady-state solution, indicating that the steady-state solutions are robust and stable. Furthermore, stable solutions are obtained during simulations of the initiation of a rock avalanche, provided that either: a small fraction of the kinetic energy of the rock fall is transferred

to internal acoustic vibrational energy; or the avalanche has a modest initial velocity. The hydrocode simulations suggest that the critical initial velocity required for a dry rock avalanche to become acoustically fluidized and develop a self-sustaining acoustic energy field is approximately 0.1 in normalized units. Using Equation 22, we see that a normalized velocity of 0.1 corresponds to $\sim 15 \text{ ms}^{-1}$, for a 10-m thick avalanche traveling down slope of 10° , where the acoustic wavelength is 0.1 m and the compressive wave speed is 100 ms^{-1} . This value is modest in comparison to eye-witness estimates of similarly large sturzstroms [Shaller, 1991, and references therein], which provides further support for the acoustic fluidization model for the mobility of sturzstroms.

5. Conclusions

Our modeling work has demonstrated that not only can acoustic fluidization increase the mobility of a dry rock

avalanche, but that, under favorable conditions, acoustic fluidization may facilitate self-sustaining motion of a dry rock avalanche, at low driving stresses (slope angles less than the angle of repose). We conclude, therefore, that acoustic fluidization is capable of explaining the extraordinary mobility of sturzstroms.

Our work predicts that, in the presence of high frequency pressure vibrations, a dry rock avalanche will “flow” with an approximately uniform effective viscosity. Although this may seem to preclude the preservation of stratigraphy during a large avalanche event, computer simulations of large rock avalanches by Campbell *et al.* [1995] show both constant viscosity flow (parabolic velocity profile) and stratigraphy preservation. Hence, bulk fluid-like flow of dry rock debris and the preservation of bulk stratigraphy should not be regarded as incompatible.

Our hydrocode modeling work has shown that an acoustically fluidized rock avalanche may reach a stable, steady state during the initiation of a rock avalanche, provided that a small fraction of the kinetic energy of the rock fall is transferred to internal acoustic vibrational energy, or the avalanche has a modest initial velocity. Furthermore, analysis of the steady-state solutions to the acoustic fluidization equations for a large, dry rock avalanche suggest that the termination of such an avalanche might be a result of the avalanche thinning to a critical limit, below which the acoustic energy field cannot sustain itself. However, because of the 1.5-D nature of our hydrocode models we have not thus far been able to accurately simulate the termination of a sturzstrom. We are currently developing SALES 2 to allow us to investigate this issue.

The study of acoustic fluidization is still in its infancy; hence, many of the model parameters discussed here have not been measured directly, or are poorly constrained. We hope to further constrain the model parameters with future work, both theoretical and experimental. Consequently, it is impossible to answer definitively whether typical sturzstrom conditions lie in the regime where acoustic fluidization could facilitate self-sustaining motion of the avalanche. In other words, whether or not acoustic fluidization is the major factor controlling the mechanics of sturzstroms. However, even with conservative estimates for the governing parameters, the acoustic fluidization model for the mechanics of sturzstroms presented here can adequately explain the high mobility of large dry rock avalanches.

Acknowledgements

Both authors contributed equally to this paper. We are grateful to Phil Shaller for access to his extensive large rock avalanche database. This research was funded by NASA grant NAG5-11493.

References

- Amsden, A. A., H. M. Ruppel, and C. W. Hirt, Sale: Simplified ALE computer program for fluid flow at all speeds, *Tech. Rep. LA-8095*, Los Alamos National Laboratory, Los Alamos, NM, 1980.
- Bagnold, R. A., The flow of cohesionless grains in fluids, *Philosophical Transactions of the Royal Society of London, A*, 225, 49–63, 1956.
- Bagnold, R. A., An approach to the sediment transport problem from general physics, *USGS Prof. Pap.*, 422I, 1–37, 1966.
- Barkan, D., *Dynamics of Bases and Foundations*, McGraw-Hill Book Company, New York, 1962.
- Brune, J. N., S. Brown, and P. A. Johnson, Rupture mechanism and interface separation in foam rubber models of earthquakes: A possible solution to the heat flow paradox and the paradox of large overthrusts, *Tectonophysics*, 218, 59–67, 1993.
- Campbell, C. S., Rapid granular flows, *Annu. Rev. Fluid Mech.*, 22, 57–92, 1990.
- Campbell, C. S., P. W. Cleary, and M. J. Hopkins, Large-scale landslide simulations: Global deformation, velocities and basal friction, *J. Geophys. Res.*, 100, 8267–8283, 1995.
- Carson, M. A., and M. J. Kirkby, *Hillslope Form and Process*, no. 3 in Cambridge Geographical Studies, Cambridge University Press, 1972.
- Chuang, F. C., and R. Greeley, Large mass movements on Callisto, *J. Geophys. Res.*, 105, 20,227–244, 2000.
- Dade, W. B., and H. E. Huppert, Long-runout rockfalls, *Geology*, 26, 803–806, 1998.
- Dainty, A. M., and M. N. Toksöv, Elastic wave propagation in a highly scattering medium—a diffusion approach, *J. Geophys.*, 43, 375–388, 1977.
- Erismann, T. H., Mechanics of large landslides, *Rock Mechanics*, 12, 15–46, 1979.
- Fineburg, J., From cinderella’s dilemma to rock slides, *Nature*, 386, 323–324, 1997.
- Frankel, A., and L. Wennerberg, Energy-flux model of seismic coda: Separation of scattering and intrinsic attenuation, *Bull. Seism. Soc. Am.*, 77, 1223–1251, 1987.
- Gaffney, E. S., and H. J. Melosh, Noise and target strength degradation accompanying shallow-buried explosions, *J. Geophys. Res.*, 87, 1871–1879, 1982.
- Goguel, J., Scale-dependent rockslide mechanisms, with emphasis on the role of pore fluid vaporization, in *Rockslides and Avalanches*, edited by B. Voight, vol. 1, pp. 693–705, Elsevier, Amsterdam, 1978.
- Heim, A., Der bergsturz von elm, *Zeitschrift der Deutschen Geologischen Gesellschaft*, 34, 74–115, 1882.
- Howard, K. A., Avalanche mode of motion: Implications from lunar examples, *Science*, 180, 1052–1055, 1973.
- Hsü, K. J., Catastrophic debris streams (sturzstroms) generated by rockfalls, *Geological Society of America Bulletin*, 86, 129–140, 1975.
- Iverson, R. M., M. E. Reid, and R. G. LaHusen, Debris-flow mobilization from landslides, *Ann. Rev. Earth Planet. Sci.*, 25, 85–138, 1997.
- Jaeger, H. M., and S. R. Nagel, Physics of the granular state, *Science*, 255, 1523–1531, 1992.
- Jaeger, J. C., and N. G. W. Cook, *Fundamentals of Rock Mechanics*, 1st ed., Chapman and Hall, 1969.
- Kanamori, H. A., Mechanics of earthquakes, *Rev. Earth Planet. Sci.*, 22, 207–237, 1994.
- Lambe, T. W., and R. V. Whitman, *Soil Mechanics, SI Version*, John Wiley and Sons, New York, 1979.
- Lucchitta, B. K., A large landslide on Mars, *Geological Society of America Bulletin*, 89, 1601–1609, 1978.
- Lucchitta, B. K., Landslides in Valles Marineris, Mars, *J. Geophys. Res.*, 84, 8097–8113, 1979.
- Malin, M. C., Mass movements on Venus: Preliminary results from Magellan cycle 1 observations, *J. Geophys. Res.*, 97, 16,337–352, 1992.
- McEwen, A. S., Mobility of large rock avalanches: Evidence from Valles Marineris, Mars, *Geology*, 17, 1111–1114, 1989.
- McSaveney, M. J., Sherman glacier rock avalanche, Alaska, U.S.A., in *Rockslides and Avalanches*, edited by B. Voight, vol. 1 of *Natural Phenomena*, pp. 197–258, Elsevier, Amsterdam, 1978.
- Melosh, H. J., Acoustic fluidization: A new geologic process?, *J. Geophys. Res.*, 84, 7513–7520, 1979.
- Melosh, H. J., Acoustic fluidization, *American Scientist*, 71, 158–165, 1983.
- Melosh, H. J., The mechanics of large rock avalanches, in *Debris Flows/Avalanches: Process, Recognition and Mitigation*, edited by J. E. Costa and G. F. Wiczeorek, pp. 41–49, Geological Society of America, 1987.
- Melosh, H. J., Dynamical weakening of faults by acoustic fluidization, *Nature*, 379, 601–606, 1996.
- Melosh, H. J., and K. K. Girdner, Rheology of vibrated granular materials: Application to long-runout landslides, *EOS*, 76, 1995.

- Reynolds, O., On the dilatancy of media composed of rigid particles in contact. With experimental illustrations, *Phil. Mag.*, *20*, 469–481, 1885.
- Richards, R., D. Elms, and M. Budhu, Dynamic fluidization of soils, *J. Geotech. Eng.*, *116*, 740–759, 1990.
- Rodger, A. A., and G. S. Littlejohn, A study of vibratory driving in granular soils, *Géotechnique*, *30*, 269–293, 1980.
- Schenk, P. M., and M. H. Bulmer, Origin of mountains on Io by thrust faulting and large-scale mass movements, *Science*, *279*, 1514–1517, 1998.
- Shaller, P. J., Analysis and implications of large Martian and terrestrial landslides, Ph.D. thesis, Caltech, 1991.
- Shingareva, T. V., and R. O. Kuzmin, Downslope movement of surface material on Phobos, in *Lunar and Planet. Sci Conf. XXXII CD-ROM*, Abs. No. 1453, 2001.
- Shreve, R. L., The Blackhawk landslide, *Geological Society of America Special Paper*, *108*, 47, 1968.
- Zik, O., J. Stavans, and Y. Rabin, Mobility of a sphere in vibrated granular media, *Europhys. Lett.*, *17*, 315–319, 1992.

G. S. Collins and H. J. Melosh, Lunar and Planetary Laboratory, University of Arizona, Tucson, AZ85721, U.S.A. Email: gareth@lpl.arizona.edu

(Received February 20, 2003.)